Science of the Total Environment xxx (xxxx) xxx

Contents lists available at ScienceDirect

Science of the Total Environment

journal homepage: www.elsevier.com/locate/scitotenv

Autonomous sensor suite for evaluating fish-turbine interactions and environmental impacts in marine renewable energy and hydropower

Aljon Salalila [a,1], Jun Lu [a,1], Jayson J. Martinez [a], Hongfei Hou [a], Zhiqun Daniel Deng [a,b,*]

[a] Energy and Environment Directorate, Pacific Northwest National Laboratory, Richland, WA 99354, USA
[b] Department of Naval Architecture and Marine Engineering, University of Michigan, Ann Arbor, MI 48109, USA

HIGHLIGHTS

- Sensor Fish devices measure aquatic life interactions with MRE systems.
- MSF, SF Mini, and FSF capture shear forces, pressure changes, and collision data.
- Field tests provide data to assess impacts and validate environmental models.
- Sensor Fish minimizes biological impacts and aids sustainable MRE system designs.

GRAPHICAL ABSTRACT

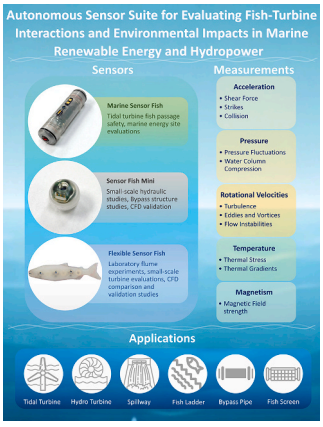

ARTICLE INFO

Editor: Damià Barceló

Keywords:
Marine renewable energy
Hydropower
Fish-turbine interactions
Ecological impacts
Sensor technology

ABSTRACT

Marine renewable energy (MRE) harnesses ocean-based resources such as waves, tides, currents, and thermal or salinity gradients for sustainable power generation. It has the potential to complement existing renewable resources, support remote communities, and contribute to decarbonization efforts. However, understanding the hydrodynamic forces created by MRE devices and their impacts on marine life is critical for responsible deployment. To address these concerns, advanced sensor devices, including the Marine Sensor Fish (MSF), Sensor Fish Mini (SF Mini), and Flexible Sensor Fish (FSF), were developed to measure interactions between aquatic organisms and MRE systems. This paper details the design, manufacturing, calibration, and field deployment of these sensor suites, highlighting their ability to capture key physical stressors such as shear forces, pressure changes, and collision impacts. The MSF successfully evaluated turbine interactions at a tidal turbine in the Salish Sea, capturing data on turbulence, collision impact, and pressure gradients. The SF Mini validated hydrodynamic conditions in scaled hydraulic models, supporting computational fluid dynamics simulations. The FSF, with its flexible silicone body, measured species-specific impacts in turbulent environments. This research

* Corresponding author at: P.O. Box 999, Richland, WA 99354, USA.
E-mail address: Zhiqun.Deng@pnnl.gov (Z.D. Deng).
[1] These authors contributed equally to this manuscript.

https://doi.org/10.1016/j.scitotenv.2025.178710
Received 12 December 2024; Received in revised form 30 January 2025; Accepted 31 January 2025

demonstrates the potential of Sensor Fish technology to advance sustainable marine energy systems by reducing biological impacts and informing environmentally sustainable designs.

1. Introduction

Marine renewable energy (MRE) technologies play a crucial role in advancing sustainable energy solutions by harnessing natural forces, such as waves, tidal currents, ocean currents, ocean thermal or salinity gradients, and large river currents. Significant potential exists in the United States to use these resources, with an estimated technical capacity of 2300 TWh per year, which is equivalent to approximately 57 % of the nation's electricity production in 2019 (Kilcher et al., 2021). MRE systems, including tidal turbines and wave energy converters, generate power by capturing the kinetic energy of moving water, thus representing a significant step toward reducing reliance on fossil fuels and mitigating climate change impacts (Garavelli et al., 2024; Copping et al., 2014). However, integrating these systems into marine environments introduces challenges, particularly concerning their potential impacts on marine ecosystems, fish populations, and biodiversity (Copping et al., 2021). As these technologies are scaled up, understanding the cumulative effects on marine biodiversity, such as the impacts of electromagnetic fields and habitat alterations, becomes increasingly important (Hemery et al., 2024; Hasselman et al., 2023). Balancing the expansion of renewable energy with the protection of aquatic ecosystems is therefore a critical concern moving forward.

MRE systems operate in dynamic aquatic environments and are subject to significant hydrodynamic forces. Key concerns include potential collisions with moving device parts, underwater noise emissions, electromagnetic fields, habitat alterations, and animal displacements. However, studies indicate these impacts are limited, with no observed entanglements or significant harm reported thus far (Garavelli et al., 2024). While early research indicates that individual devices pose minimal risks, such as low collision likelihood and limited habitat disruption, ongoing studies are essential to understand interactions across species and environmental conditions. The ability of aquatic organisms to detect, avoid, or interact with these systems remains uncertain, with responses likely varying by species and environmental context (Copping et al., 2023). As the industry scales up and larger arrays potentially altering local ecosystems, continued research will be crucial to identifying and mitigating unforeseen ecological impacts (Garavelli et al., 2024).

One of the primary concerns associated with MRE development is the risk of fish colliding with moving parts, particularly the rotating blades of tidal, riverine, and ocean current turbines (Copping et al., 2021). Various studies have estimated the probability of fish encountering turbine blades to be very low (Copping et al., 2023; Shen et al., 2016; Peraza and Horne, 2023), and controlled experiments have shown that fish can modify their swimming trajectory to avoid collisions (Amaral et al., 2015; Bender et al., 2023; Yoshida et al., 2022). However, even a small number of fish lost to collisions with turbines could have detrimental effects on threatened and endangered species making a better understanding of the risk is necessary. Collisions (i.e., strike events) remain difficult to observe in natural settings due to the high turbulence and low visibility of the water where energy turbines are often deployed (Copping et al., 2014; Cotter and Staines, 2023). Nevertheless, a recent study with optical cameras mounted on a riverine turbine recorded some collisions of sockeye salmon smolt with the rotating turbine blades and a large majority of behavioral avoidance or near-miss evasions. However, the outcomes of these collisions and evasions were unknown (Courtney et al., 2022). Advanced controlled experiments with fake fish equipped with sensors (i.e., sensor fish) sent on a collision path with turbine blades would enable greater understanding of the various stresses that fish may experience as they approach, and potentially hit, a rotating turbine blade.

To address these concerns, advanced sensor devices such as the Marine Sensor Fish (MSF), Flexible Sensor Fish (FSF), and Sensor Fish Mini (SF Mini) have been developed to monitor and assess interactions between MRE systems and aquatic organisms (Deng et al., 2014; Salalila et al., 2019; Deng et al., 2024). Originally designed to study the impact of hydropower, the Sensor Fish (SF) is an autonomous device equipped with multiple sensors that measure the physical stressors fish experience as they pass through or near hydropower turbines and, more recently, MRE structures. These stressors include hydrodynamic forces such as shear, strikes, pressure changes, and turbulence that may cause injury or mortality in fish. For instance, during turbine passage, juvenile fish such as salmon may experience barotrauma from rapid pressure changes, causing severe internal injuries, such as ruptured swim bladders, and increasing mortality rates (Richmond et al., 2014; Brown et al., 2014). By using SF, researchers have been able to capture high-resolution data on the environmental conditions fish encounter as they move through hydropower turbines or MRE systems, allowing detailed assessment of potential biological impacts. For example, in a study assessing low-head hydropower turbines (Boys et al., 2018), the authors used SF to evaluate three different turbine types (i.e., very low head, Archimedes screw, and horizontal Kaplan turbines) and observed variations in pressure and strike risks depending on the turbine design, providing insights into optimizing technologies to reduce fish injury during passage. Similarly, another study employed the SF at the Nam Ngum Dam in the Mekong River to characterize hydraulic conditions within Francis turbines, comparing the physical stressors to other turbines worldwide and highlighting the hydraulic challenges specific to tropical fish species (Martinez et al., 2019a).

In a study investigating turbine design improvements, SF was used to evaluate the performance of a new turbine design at Wanapum Dam. The authors demonstrated that modifications to blade shape significantly improved fish passage survival by reducing turbulence and pressure changes during turbine operation (Deng et al., 2010). Similar assessments of Kaplan turbines were conducted at Ice Harbor Dam, using SF to document differences in nadir pressures and collision rates, which informed the development of fish-friendly design features for future turbine replacements (Martinez et al., 2019b). Finally, at the Xayaburi Hydropower Plant, SF data were combined with computational fluid dynamics (CFD) models to validate hydraulic conditions, demonstrating the value of integrating physical data with simulations to predict fish passage outcomes (Romero-Gomez et al., 2024a).

Building on prior applications, this study aims to address the overarching goal of minimizing the biological and ecological impacts of MRE and hydropower systems on aquatic species. To achieve this, the research focuses on the following key tasks: (1) designing, manufacturing, and calibrating three advanced sensor devices: the MSF, SF Mini, and FSF; (2) evaluating their performance through controlled laboratory experiments and field deployments to capture key hydrodynamic stressors such as shear forces, pressure changes, and collision impacts; and (3) demonstrating how the data collected from these devices can be used to inform future CFD model validation and support turbine design improvements. By leveraging innovative sensor technology, this research provides valuable insights into fish-turbine interactions, supporting fish passage safety and the development of environmentally sustainable energy technologies.

2. Material and methods

2.1. Design and manufacturing

Following the development of the original SF (Deng et al., 2014),

several specialized variants have been designed to address specific research needs in different hydrodynamic environments. The MSF was developed to study the interactions of marine animals with MRE technologies, such as tidal turbines (Fig. 1a). Building on the core capabilities of the original SF, the MSF includes a salinity sensor to measure total dissolved salt content in ocean water, making it ideal for capturing critical environmental data in marine settings. It also includes an acoustic transmitter that emits a coded signal at 416.7 kHz with a source level of 160 dB (Lu et al., 2016), facilitating three-dimensional (3D) localization as it navigates complex marine energy systems.

The SF Mini was developed and optimized as a compact alternative for small-scale hydraulic structure models and reduced-scale physical testing (Fig. 1b), with a spherical design measuring 23 mm in diameter and weighing 6.4 g. Despite its smaller size, the SF Mini maintains high-resolution data capture with a 2048 Hz sampling rate across its core sensors. However, to achieve its reduced form factor, the SF Mini excludes several components present in the SF, such as the temperature sensor, program board, download board, and radio-frequency (RF) transmitter. This omission minimizes its power consumption and size while still enabling comprehensive measurements through its digital 200 g accelerometer, 4000°/s gyroscope, and high-precision pressure sensor. For buoyancy control and recovery, the SF Mini can be equipped with a self-inflating balloon tag instead of relying on a mechanical weight release mechanism.

The SF Mini has two additional variants: the SF Mini-Cluster (Fig. 1c) and the SF Mini-Flat (Fig. 1d). The SF Mini-Cluster features a three-axis pressure sensor for 3D mapping of the hydraulic environment, providing detailed pressure distribution data for complex flow scenarios. In contrast, the SF Mini-Flat is a specialized version designed to attach directly to turbine blades, measuring the hydrodynamic forces on the blade surfaces and contributing to a deeper understanding of fluid-structure interactions within turbine systems.

The FSF, a variant of the SF Mini, is designed to replicate the physical form of various aquatic species, including salmon, shad, eels, and orcas (Fig. 1e). Constructed from flexible silicone and embedding the same core printed circuit board (PCB) and sensors as the SF Mini, the FSF closely resembles the texture and shape of these species. Sensors are distributed throughout the head, mid-body, and tail, allowing precise measurements of physical stresses experienced by different parts of the body. This configuration enables the FSF to accurately capture shear forces, pressure impacts, and strike events on flexible body structures, providing a better understanding of species-specific responses to hydraulic conditions and interactions with small-scale hydrodynamic systems. An overview of the original SF, MSF, SF Mini, and FSF is provided in Table 1.

2.1.1. Sensor integration and hardware architecture of the MSF, SF Mini and FSF devices

2.1.1.1. MSF description. The MSF is a versatile autonomous device designed to collect high-resolution data in diverse marine environments, such as tidal turbines and other MRE systems. It is equipped with a digital-output, three-axis microelectromechanical system (MEMS) gyroscope with a full-scale range of ±2000°/s per axis. The gyroscope uses three integrated 16-bit analog-to-digital converters for precise data digitization and features a user-selectable low-pass filter with an I2C interface, allowing flexible data acquisition. Centrally mounted on the circuit board, the gyroscope is aligned with the device's center of mass for optimal accuracy. For high-impact applications, an extended-range gyroscope (±4000°/s) is available to capture critical data during rapid rotations or high-speed impacts.

Accompanying the gyroscope is an ultra-low-power three-axis MEMS accelerometer with a full-scale range of ±200 g per axis. Like the gyroscope, the accelerometer is mounted near the center of the circuit board. It offers user-selectable bandwidths from 60 Hz to 2560 Hz, allowing users to tailor its configuration for specific hydrodynamic conditions. Additionally, the MSF integrates a high-precision pressure sensor rated for a full-scale range of 12 bars and an overpressure tolerance of 30 bars, making it suitable for deployment in deep-water applications. The temperature sensor operates across a broad range of −40 °C to +125 °C, assuring reliable environmental data in various marine conditions.

The entire sensor suite is built onto a thin, multilayer PCB that houses the sensors and is powered by a compact lithium-polymer battery, all enclosed in a durable polycarbonate housing. This compact, integrated design enhances the robustness of the MSF in high-pressure and turbulent environments while minimizing potential points of failure. A 3D rendering of the MSF (Fig. 2a) illustrates its key components, highlighting the PCB layout and sensor arrangement. A photograph of the completed device is shown in Fig. 2b, providing a visual representation of its final deployment form factor and size. The hardware architecture, shown in Fig. 2c, provides a comprehensive overview of the internal layout, detailing the sensor connections, power management, and communication interfaces.

To facilitate device recovery after data collection, the MSF features a spring-loaded weight release mechanism and a built-in RF transmitter. Upon completion of data recording, the weight is released, and four high-intensity orange light-emitting diodes (LEDs) and the RF transmitter are activated periodically, making the MSF highly visible and traceable using RF receivers. Additionally, the MSF can be equipped with a self-inflating yellow balloon tag (Heisey et al., 1992; Salalila

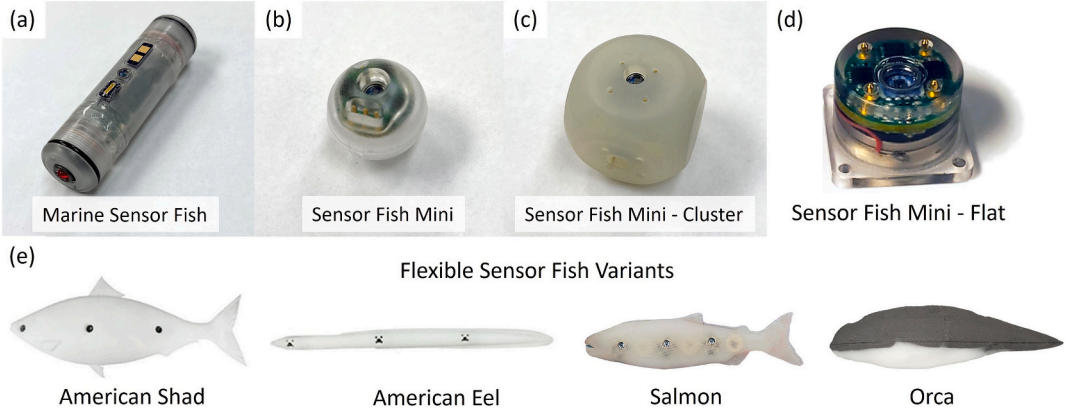

Fig. 1. Photographs of SF variants. (a) MSF designed for studying MRE technologies. (b) SF Mini for investigating hydraulic structure models at smaller scales. (c) SF Mini–Cluster is equipped with a three-axis pressure sensor for precise mapping of pressure variations. (d) SF Mini–Flat tailored for mounting on hydraulic blades to analyze hydrodynamic forces. (e) FSF models equipped with embedded sensors in the head, mid-body, and tail sections, designed to represent species such as the American Shad, American Eel, Salmon, and Orca for species-specific studies.

Table 1
Overviews of the original SF, MSF, SF Mini, and FSF.

Device type	Description	Dimensions & weight	Sensors	Applications	Application examples
Original SF	Autonomous device mimicking juvenile salmon to measure physical stressors in hydraulic environments. Widely used in dam studies and commercially available from ATS.	Diameter: 24.5 mm, Length: 89.9 mm, Weight: 42.1 g	3D gyroscope, 3D accelerometer, 3D magnetometer, pressure sensor, temperature sensor, RF transmitter	Evaluates pressure changes, shear stress, and collision risks in hydropower systems.	Hydropower dam impact studies, fish passage assessments, historical data comparison for future studies.
MSF	Designed to study marine animals' interactions with energy systems such as tidal turbines in marine environments.	Diameter: 24.5 mm, Length: 89.9 mm, Weight: 42.1 g	Salinity sensor, 3D gyroscope, 3D accelerometer, pressure sensor, temperature sensor, RF transmitter, acoustic transmitter	Assesses interactions with tidal turbines and other marine energy technologies.	Tidal turbine fish passage safety, MRE site evaluations.
SF Mini	Compact version for reduced-scale testing and small hydro deployments in low-flow conditions.	Diameter: 23 mm, Weight: 6.4 g	3D gyroscope, 3D accelerometer, pressure sensor	Suitable for smaller hydraulic models, low-flow conditions, and CFD modeling validation.	Laboratory flume tests, small-scale turbine evaluations, CFD comparison and validation studies.
FSF	Silicone-based design using the SF Mini board to mimic aquatic animals like salmon, shad, eel, seal, and orca.	Varies by model	3D gyroscope, 3D accelerometer, pressure sensor	Assesses shear stress, pressure fluctuations, and strike impacts in smaller hydraulic systems.	Bypass structure studies, small-scale hydraulic tests, flume tank experiments, MRE device evaluations.

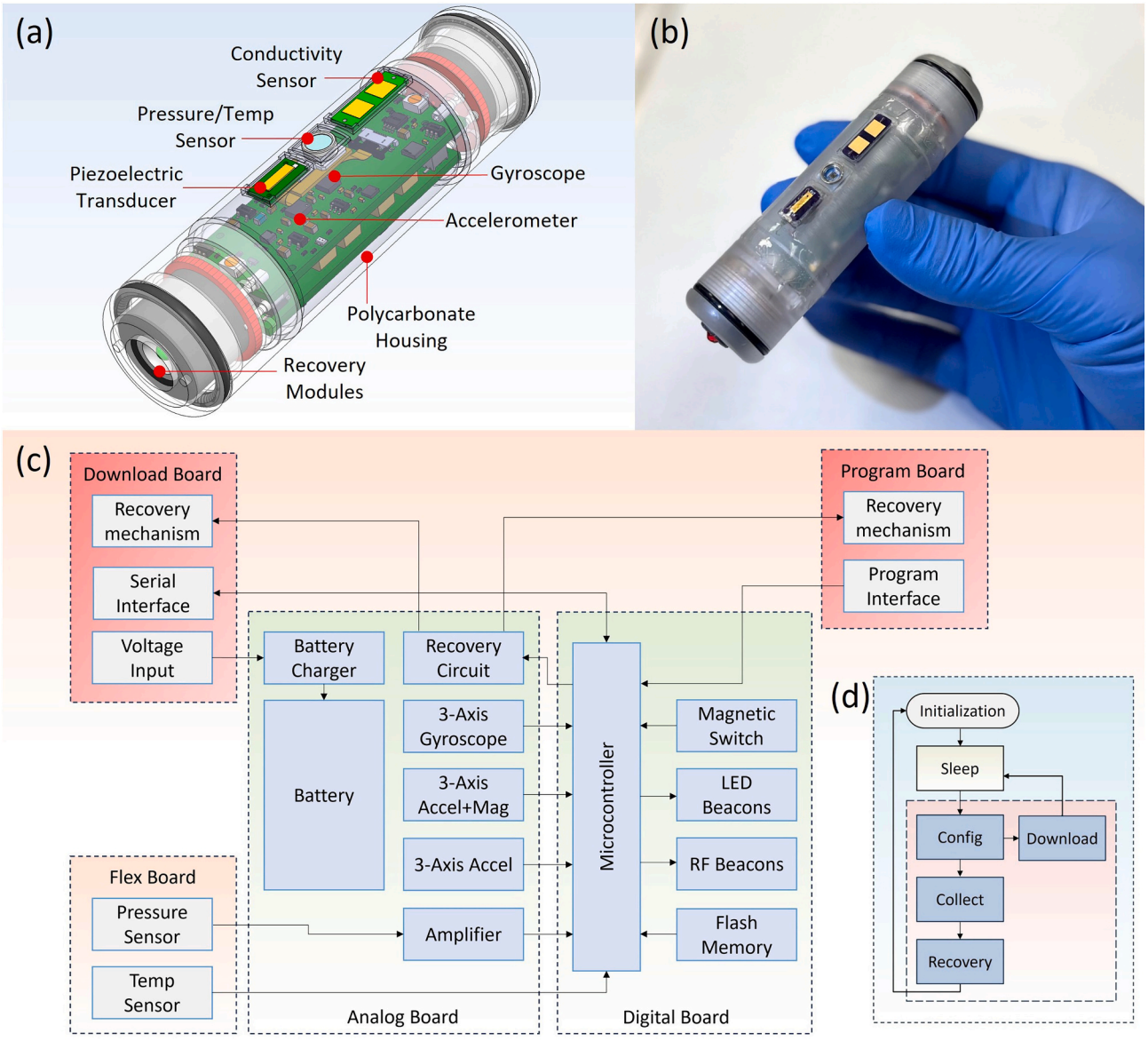

Fig. 2. Schematic illustrations and photograph of the MSF. (a) 3D rendering of the MSF, highlighting its key components, including the thin multilayer PCB with sensors, all enclosed in a polycarbonate housing. (b) Photograph of the device. (c) Hardware architecture of the MSF. (d) Simplified flowchart of the firmware.

et al., 2023), which improves visibility and assists the retrieval crew in locating the device in open-water environments.

To enhance its hydrodynamic stability during deployment, all MSF components are strategically placed to align the center of gravity of the device with its geometric center. Its balanced design is critical for maintaining steady motion in turbulent environments, assuring data integrity and repeatability during high-impact interactions.

2.1.1.2. Firmware functionality and operational states. The MSF firmware manages multiple operating modes, ensuring smooth transitions between initialization, data acquisition, and recovery. The simplified firmware flowchart shown in Fig. 2d outlines the main operational states of the device, including configuration, active data collection, and recovery. During the manufacturing process, the firmware is uploaded for setup. Essential parameters, such as delay time and data collection duration, are set to default values at this stage. Once configured, the MSF enters a low-power sleep mode to conserve energy until a configuration interrupt is triggered via a cable connection. Upon detecting this interrupt, the MSF transitions to an active state and awaits serial commands to either download collected data or modify configuration parameters, such as data sampling rate and recording intervals, in preparation for future deployments.

When set for data collection, the MSF is activated using a magnetic switch and deployed into the marine environment, recording data at a sampling rate of 2 kHz. After data collection is complete, the recovery function is triggered, which releases the weight and activates the RF transmitter for efficient retrieval. If a self-inflating balloon tag is included in the configuration, it automatically inflates after the device exits the tested hydraulic structure, providing a visual aid for locating the device. Upon successful recovery, the MSF returns to its low-power sleep mode, preserving battery life until it is reconnected for data download and reconfiguration.

2.1.1.3. Comparison to other SF variants. The SF Mini and FSF share many core features and sensors with the MSF, such as the three-axis MEMS gyroscope, three-axis accelerometer, and high-precision pressure sensor. However, the SF Mini and FSF lack several key components found in the MSF, including the temperature sensor, program board, download board, and RF transmitter. These omissions are intentional, as the SF Mini is specifically designed for smaller-scale applications and controlled environments, such as laboratory flume tests, scaled hydraulic model evaluations, and CFD validation studies. The configuration of the SF Mini is more compact and streamlined, making it ideal for detailed hydrodynamic measurements in indoor test facilities or prototype evaluations where the extended functionality of RF transmitters or temperature monitoring is not essential.

The hardware architecture of the SF Mini uses the same PCB, lithium battery, and polycarbonate housing as the FSF. However, unlike the FSF, which is embedded in a silicone-based flexible body to measure shear forces and strike impacts, the SF Mini retains a rigid, spherical shape, making it well-suited for capturing acceleration, rotational velocity, and pressure data in compact spaces and scaled-down hydraulic systems. This allows the SF Mini to act as a surrogate for live fish in scenarios where physical prototypes are tested before full-scale implementation. For example, the SF Mini was used in a comparative CFD study to collect high-resolution hydrodynamic data in a test rig that simulated fish passage conditions in a Kaplan turbine (Romero-Gomez et al., 2024b). The data were then compared to computational simulations to validate the accuracy of the CFD models, thus ensuring the simulated flow fields matched the actual measurements.

Additionally, the SF Mini has been deployed in smaller hydraulic structures, such as the bypass channel of the Davenport Farmers Screen, to measure the impact of flow conditions on fish passage efficiency and safety (Salalila et al., 2019), demonstrating the use of both the SF Mini and the original SF to validate CFD models, and providing insights into the hydraulic performance and fish passage conditions of these systems. This approach of using physical data to cross-check CFD predictions has proven critical for refining design features and ensuring fish-friendly conditions in existing and future structures.

The SF Mini is designed without a temperature sensor, program board, or RF transmitter, minimizing its size and power consumption, making it more cost-effective and easier to deploy than the original SF and MSF. Instead of using a program board to trigger a tungsten weight release for buoyancy, the SF Mini can be equipped with self-inflating balloon tags to aid in recovery after data collection, eliminating the need for additional mechanical components. This design allows the SF Mini to leverage its core sensors—including a digital 200-g, 12-bit accelerometer, 4000°/s gyroscope, and high-precision pressure sensor—to collect high-quality data in constrained spaces where larger devices, such as the MSF, cannot be deployed effectively. Consequently, while the MSF is equipped for comprehensive, long-term data collection with additional features such as an acoustic transmitter, salinity sensor, and a larger 256 Mbit flash memory, the SF Mini and FSF—using the same core sensors and housing—offer specialized solutions for smaller-scale, indoor applications such as validating design concepts in hydraulic models and conducting CFD simulations. A detailed comparison of the sensor specifications and hardware configurations for all four devices is presented in Table 2.

2.1.2. Manufacturing process of the MSF, SF Mini and FSF devices

2.1.2.1. MSF. Manufacturing the MSF involves a series of assembly steps to ensure reliable performance in harsh marine environments. The process begins with the preparation and assembly of the circuit boards, which includes separating the analog and digital boards from the circuit board panel. They are carefully separated using needle-nose pliers and visually inspected for defects. Any defective or incomplete boards are discarded to maintain quality standards. Once the boards pass inspection, the battery attachment step begins. The surface of the analog board and the 3.7 V lithium polymer battery are cleaned thoroughly with isopropyl alcohol to promote proper adhesion. A thin layer of epoxy is applied to the battery surface using a toothpick after which the battery is carefully positioned onto the analog board and secured in place with a rubber band until the epoxy cures. Then, the battery wires are trimmed and soldered to the board's power pads.

For the digital board, integrating the antenna is a critical step. A 10-in. antenna wire is cut and soldered to the designated port on the digital board. The antenna wire is routed around key components to minimize interference and is secured with ultraviolet glue that is cured using an ultraviolet LED system. After assembling the key electronic components, the MSF undergoes initial power testing. A power supply is connected to charge the battery, and the battery's status is verified using an LED indicator. If the battery is fully charged, the LED shows a green light, signaling readiness for the next phase, which involves programming and configuration. During this phase, the digital board is connected to a 3 V power supply, and a radio scanner is used to identify and log potential frequencies emitted by the board. Once the correct frequency is located and verified using a radio receiver, it is marked on the board for future reference.

Firmware is then uploaded using MPLAB X IDE software. The microcontroller on the analog and digital boards is programmed by connecting a microchip programmer to the designated port. After firmware installation, the RF transmitter is tested with a radio receiver to ensure proper functionality. The device is then evaluated using the SF Communicator software. This software is used to configure the device's settings, download data, and visualize recorded measurements, ensuring all functionalities are operating correctly.

When the electronic components are functioning properly, the next step is housing preparation and sensor integration. Shallow cuts are made on the contact surfaces of the main housing and end caps with a

Table 2
Comprehensive comparison of sensor specifications and hardware configurations for the original SF, MSF, SF Mini, and FSF.

Specification	Original SF	MSF	SF Mini	FSF
Acceleration	Analog 200-g, 12-bit oversampling at 8192 samples/s	Digital 200-g, 12-bit sampling at 2048 samples/s	Digital 200-g, 12-bit sampling at 2048 samples/s	Digital 200-g, 12-bit sampling at 2048 samples/s
Pressure	12-bit oversampling at 8192 samples/s	12-bit oversampling at 8192 samples/s	12-bit oversampling at 8192 samples/s	12-bit oversampling at 8192 samples/s
Gyroscope	2000°/s	4000°/s	4000°/s	4000°/s
Magnetometer	Digital ±8.1 gauss	Digital ±16 gauss	None	None
Salinity sensor	N/A	Integrated	N/A	N/A
Acoustic transmission	N/A	Integrated	N/A	N/A
Temperature sensor	−40 to +125 °C	−40 to +125 °C	N/A	N/A
RF transmitter	Integrated	Integrated	None	None
Flash memory	128 Mbit, 2.7 V to 3.6 V	256 Mbit, 2.7 V to 3.6 V	128 Mbit, 2.7 V to 3.6 V	128 Mbit, 2.7 V to 3.6 V
Battery	110 mAh Li	110 mAh Li	63 mAh Li	63 mAh Li
Recording time	292 s	584 s	292 s	292 s
Data communication	Wired speed 961,200 bps	Wired speed 961,200 bps	Wired speed 961,200 bps	Wired speed 961,200 bps
Housing material	Polycarbonate	Polycarbonate	Polycarbonate	Polycarbonate, embedded in flexible silicone housing
Recovery mechanism	Spring-loaded tungsten weight release, RF transmitter	Spring-loaded tungsten weight release, RF transmitter, and self-inflating balloon tag option	Self-inflating balloon tag (optional, since no download/program board to trigger tungsten weight release)	Self-inflating balloon tag (optional, because no download/program board to trigger tungsten weight release)

razor blade to improve epoxy adhesion, and painter's tape is applied to mask areas where epoxy is not needed. The main housing and end caps are masked with painter's tape, and shallow cuts are made on the contact surfaces with a razor blade to help the epoxy bond better. The pressure sensor is carefully mounted using epoxy applied around its base, and the sensor is inserted into the housing port. To achieve a secure fit, additional epoxy is applied around the sensor attachment point and evenly spread. More epoxy is used to fill any gaps, creating a watertight seal around the pressure sensor. After the epoxy cures, the tape is removed, and the housing is cleaned thoroughly to eliminate any residual adhesive.

The final assembly stage involves carefully inserting the assembled circuit board into the prepared housing. The board must be aligned precisely with the pressure sensor port to ensure proper functionality. Once positioned, the program and download end caps are attached to the housing, and epoxy is applied to both the inner and outer surfaces of the housing-to-endcap interface. The assembly is then placed on a resting rack to cure for 24 h, ensuring all seals are secure and the device is watertight.

2.1.2.2. SF Mini. Manufacturing the SF Mini involves several detailed steps aimed at ensuring optimal functionality and durability. The process starts with soldering the 3.7 V lithium battery to the PCB (Fig. 3a). The battery must be checked using a multimeter to make sure it reads between 3.5 V and 3.7 V. Solder flux is applied to both the battery pins and the VCC and ground receptacles on the PCB to improve adhesion. Once the positive and negative terminals of the battery are properly aligned with the VCC and ground ports, they are soldered into place. After soldering, the battery connection is confirmed by gently tugging it to make sure the fit is secure.

The next step involves uploading the firmware to the PCB using MPLAB X IDE software. The serial number is updated, and the firmware is compiled and loaded onto the microcontroller. A connection between the RS232 programming cable and the PCB ensures proper communication during programming.

Once the PCB is prepared, it is detached from the circuit board panel (Fig. 3b), and LOCTITE adhesive is applied to secure the PCB to the top housing of the SF Mini (Fig. 3c–d). After allowing the adhesive to cure, epoxy is applied around the pressure sensor to create a water-tight seal. To make sure the top and bottom housing components bond securely, crisscross slices are applied using an X-Acto knife. These slices increase the surface area, thus enhancing the epoxy's ability to hold the two parts together.

To finalize the assembly, the mass of the SF Mini is tuned to achieve neutral buoyancy. This is done by applying small amounts of epoxy to the inner walls of the housing, making sure that both the top and bottom halves weigh 3.2 g each. Once the desired mass is achieved, the final assembly step involves joining the top and bottom housing components with adhesive (Fig. 3e). Excess adhesive is removed, and the SF Mini is left to cure for 24 h, resulting in a fully assembled unit that is ready for calibration. The download cable, made from receptacle pins and RS232 3.5 V cables, is housed in a 3D-printed resin material and is used for programming the SF Mini and downloading data from it (Fig. 4f-g).

2.1.2.3. FSE. The design and manufacturing process for the Flexible Sensor Eel (FSE) follows a detailed and structured approach that can be adapted for various target species, including shad, orca, and salmon. This adaptability makes the process versatile for different environmental applications while maintaining consistency in the core procedures. The same general approach is used for each species, with modifications based on their unique anatomical features and use cases for each target.

The first step in creating the FSE is the selection of the target species, which in this case is the American Eel. A 3D model of the eel is developed to capture the essential dimensions, including length, width, and girth, providing an accurate physical representation. This model serves

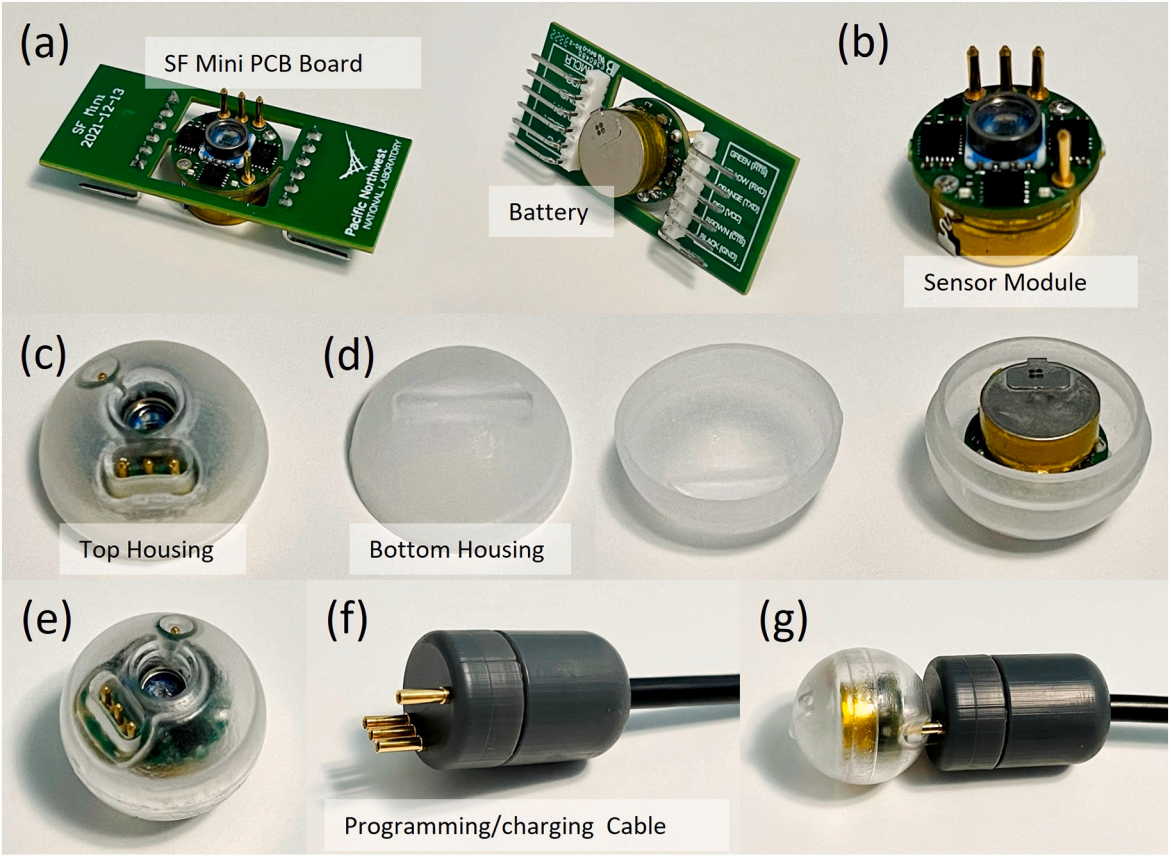

Fig. 3. High-level overview of the SF Mini manufacturing procedure. (a) Solder lithium battery and load firmware onto PCB. (b) Break away the sensor module assembly from the PCB panel. (c) Attach sensor module to housing. (d) Balance top and bottom housing with epoxy. (e) Attach top and bottom housing together. (f) Solder receptacle pins to RS232 3.5 V cables and epoxy programming/downloading housing. (g) SF Mini connected to the programming/downloading cable.

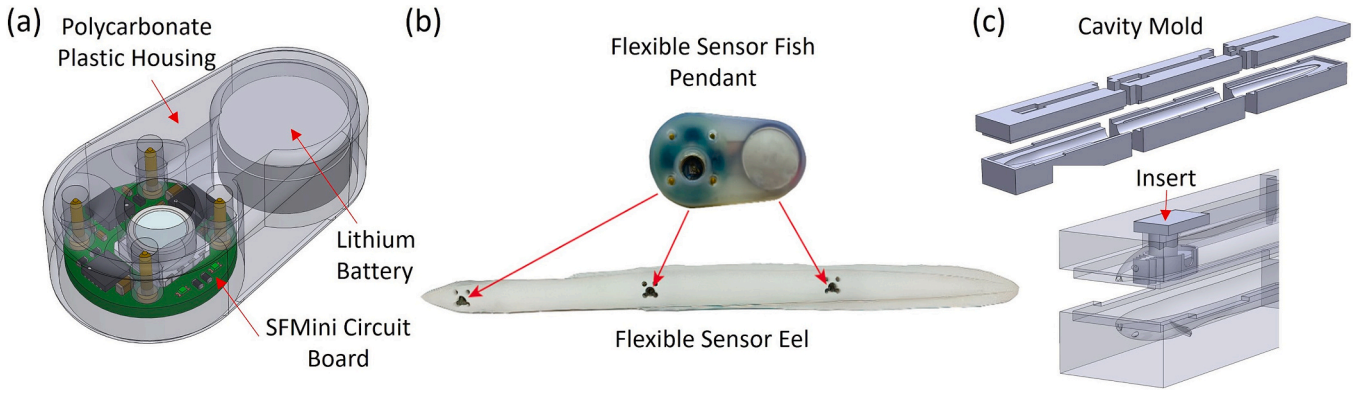

Fig. 4. Manufacturing method of the Flexible Sensor Eel (SFE). (a) 3D rendering of the FSF Pendant, highlighting its key components, including the thin multilayer PCB with sensors, a lithium battery, and a polycarbonate housing sealed in epoxy. (b) Photograph of the FSF Pendant and the FSE, showing where it was embedded in the eel's body. (c) Exploded view of the FSE cavity mold, indicating the placement location for the insert prior to molding.

as the foundation for the design and is iterated upon with input from partners to confirm that the dimensions align with the intended specifications. The same 3D modeling approach is used for other species such as shad, orca, seal, and salmon.

The sensing hardware for the FSE is based on the SF Mini architecture, but it has been reconfigured into a form factor better suited for the eel's slim body (Fig. 4a). This new version, referred to as the FSF Pendant, moves the battery to the side of the circuit board and sensors, thereby reducing the overall profile of the device (Fig. 4b). The PCB and sensing components are then housed in a polycarbonate enclosure that is sealed with epoxy to protect the electronics while still allowing access to the pressure sensor and data/charging pins. The FSF Pendant is calibrated using the same methodology employed in the SF Mini devices. This reconfiguration of the hardware is essential to make sure it fits within the thin, flexible body of the eel while still performing the necessary data collection functions. The same process applies to shad, orca, seal, and salmon designs, with variations in the sensor housing tailored to their specific body shapes.

The primary material for the FSE body is a platinum-cure silicone, specifically Smooth-On Dragonskin 10 Medium. This flexible material allows the FSE to mimic the natural movement of an eel in water while protecting the internal sensors. A mold is created based on the 3D model

of the eel, with a cavity included for housing the FSF Pendant. The mold is 3D-printed in PLA, allowing for quick iterations, easy modification, and low-cost production (Fig. 4c). Because of the eel's elongated shape, the mold is printed in sections that fit together using interlocking teeth and channels. This approach enables proper alignment during the curing process, and the same molding approach is used for other species, regardless of their body shape.

To account for buoyancy, glass microbubbles are mixed into the silicone, which brings the FSE body closer to neutral buoyancy in water. These microbubbles are also used in the fabrication of shad, orca, seal, and salmon models, with the proportion adjusted based on the size and density of the target species.

A final key step in the process is the application of SLIDE Surface Tension Diffuser (SLIDE STD), which reduces the surface friction of the silicone body. This additive is mixed into the silicone before molding and creates a smooth, low-friction surface once the body has fully cured. For the FSE, the entire body is poured in SLIDE STD silicone in a single step, ensuring consistency throughout the structure. Larger species, such as orca or salmon, may require multiple pours, but the overall methodology remains the same across different models. The final curing process for SLIDE STD silicone involves a 24-h air cure to fully develop its low-friction properties, a step that applies universally to all species implementations.

The design and manufacturing process for the FSE is a streamlined yet flexible approach that can be applied to various species. The core procedures, ranging from 3D modeling to sensor housing design, silicone molding, and surface finishing, remain consistent, with only minor modifications needed to account for the specific anatomical characteristics of each target species.

2.2. Sensor calibration

The MSF undergoes a calibration process to enable accurate measurements from its integrated gyroscope, accelerometer, pressure, and temperature sensors. The MSF Controller application is used to program the MSF with specific settings such as recording time and delay time and is used for downloading and visualizing the recorded data. This same calibration method is applied to the SF Mini and FSF variants, which share similar core sensor configurations. The MSF Calibration software, developed in MATLAB, is then used to process raw data from each sensor and calculate the necessary offset and scaling values for calibration.

The gyroscope calibration begins by setting up the MSF with a 5-s delay and a 60-s recording time using the MSF Controller application. During calibration, the device is placed on a stable surface to minimize external vibrations. Fig. 5a shows the internal sensor orientation of the MSF and how the acceleration and rotational velocity directions are aligned. After recording, data are downloaded and analyzed using the MSF Calibration software to determine offsets for each axis. These values are saved in a calibration file and verified through an acceptance test by mounting the MSF on an Angular Speed Simulation Rig (Fig. 5b). The rig starts at 0°/s and systematically increases to 2000°/s in increments, rotating clockwise first and then counterclockwise. The recorded data is compared against known values to ensure calibration accuracy. The gyroscope calibration is considered successful if the relative error is less than 5 % for each axis.

For accelerometer calibration, the MSF is programmed with a 5-s delay and 40-s recording time. It is then placed on the Accelerometer Test Track (Fig. 5c) and released to collide with a stopper, generating acceleration peaks of around 95 g. Five repetitions are conducted for verifying consistency. The MSF Calibration software is used to calculate

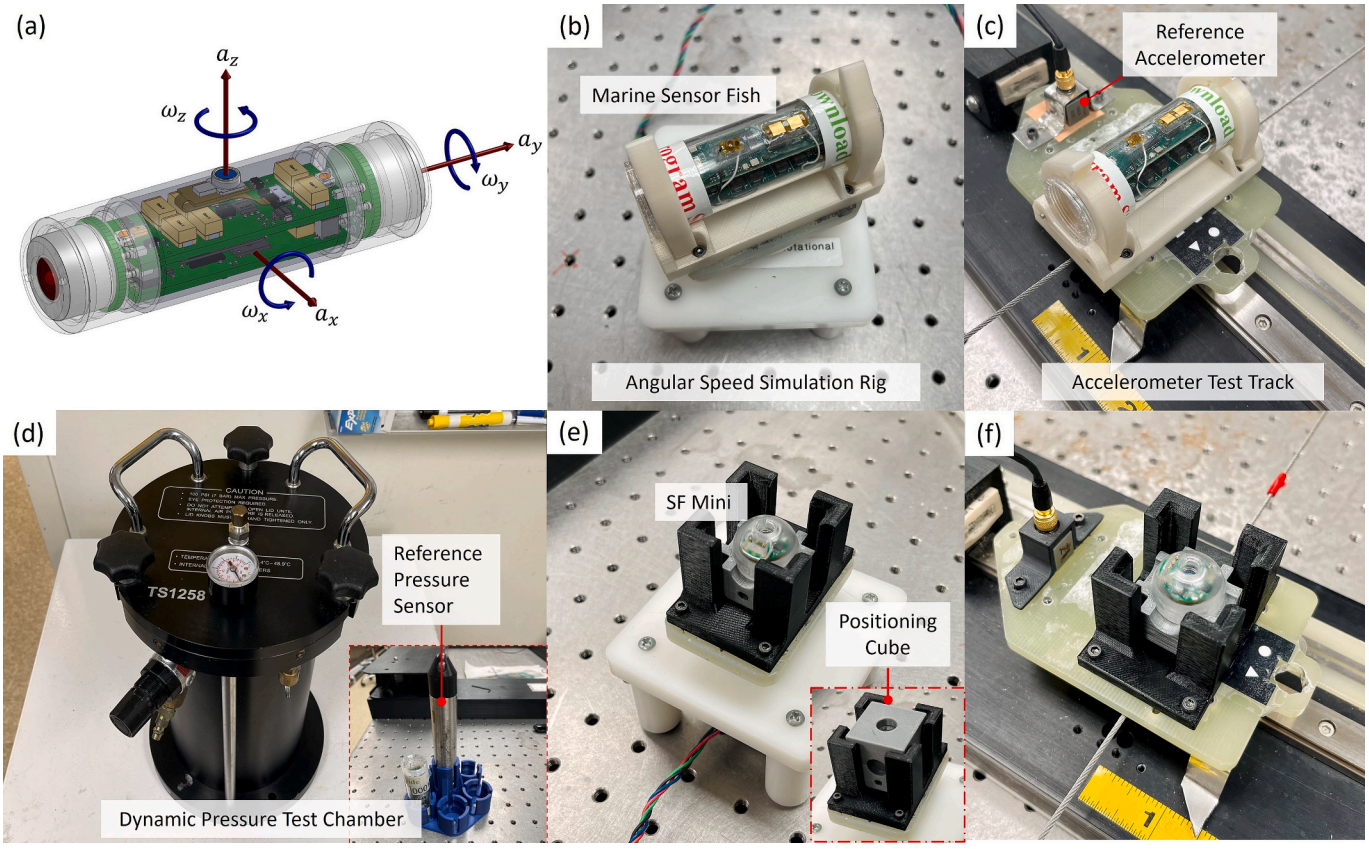

Fig. 5. High-level overview of the calibration setups for the MSF and SF Mini. (a) Visualization of acceleration and rotational velocity directions based on the internal sensor orientation in the MSF. (b) MSF on Angular Speed Simulation Rig for gyroscope calibration. (c) MSF on Accelerometer Test Track. (d) MSF with reference pressure sensor next to the Dynamic Pressure Test Chamber. (e) SF Mini inside the Positioning Cube on the Angular Speed Rig. (f) SF Mini on Accelerometer Test Track with a reference accelerometer.

the necessary scaling factors and offsets by comparing the MSF data to that of a reference accelerometer. The process is validated through repeated testing to confirm a relative error below 5 %.

Pressure sensor calibration is conducted using a Hobo pressure sensor in a controlled pressure chamber. Both sensors are mounted together in a Dynamic Pressure Test Chamber setup (Fig. 5d), and the chamber is gradually pressurized up to 552 kPa. The Hobo sensor serves as a reference, and the MSF Calibration software uses the collected data to derive calibration coefficients. The calibration is confirmed when the linear regression achieves a coefficient of determination (R^2) close to 1.

Temperature sensor calibration, which applies only to the MSF, involves submerging the device in an ice-water mixture to establish a reference point at 0 °C. After a 5-min stabilization period, a 30-s dataset is recorded. The MSF Calibration software processes the raw temperature data to determine offset and scaling values. This step is repeated to verify the sensor's accuracy within the operating range of −40 °C to +125 °C, with an acceptance threshold of less than 5 % error.

For the SF Mini, calibration setup follows a similar procedure. The SF Mini is mounted inside a Positioning Cube on the Angular Speed Simulation Rig (Fig. 5e) during gyroscope calibration and on the Accelerometer Test Track with a reference accelerometer for accelerometer calibration (Fig. 5f).

2.3. Test sites and setup description

2.3.1. MSF field validation

The field study was conducted at the University of Washington's (UW) tidal turbine site (Polagye et al., 2024), located in the Sequim Bay channel, WA (Fig. 6a). The turbine, measuring 1.19 m in height with a rotor diameter of 0.85 m, was mounted on a lander structure standing 1.35 m tall. This configuration positioned the rotor's top approximately 2.7 m above the seabed, at a depth of 6.2 m at mean low-low water. The turbine was situated in a navigational channel, making it essential to design the experimental setup to minimize interference with vessel traffic while collecting accurate data.

To enable precise tracking of MSF trajectories around the turbine, we deployed a three-dimensional (3D) localization array using six stationary Juvenile Salmon Acoustic Telemetry System (JSATS) receivers (Weiland et al., 2011), as depicted by the green dots in Fig. 6a. The receivers were anchored at the corners of a nominal hexagon surrounding the turbine (yellow dot). The deployment and recovery vessels were stationed near the array, represented by the red and blue dots, respectively, to facilitate the release and retrieval of the MSFs during the study. The positioning of the receivers was determined through an analysis of the natural topography, providing optimal coverage for accurate time-of-arrival data to compute high-resolution 3D positions of the MSFs as they drifted through the study area.

The acoustic receiver assembly (Fig. 6b) included a hydrophone attached to the top of the receiver unit, which was mounted on a mooring line equipped with a polyethylene fin to reduce drag. Intermediate floats were attached along the buoy line to maintain stability and proper depth alignment. The mooring lines terminated in steel anchors, selected based on the local water velocity and substrate characteristics, to ensure secure placement. In high-velocity areas, heavier, disk-shaped anchors were used to prevent displacement, while lighter, brick-style anchors were used in low-velocity zones. Wire rope was employed instead of nylon in areas prone to abrasion, providing additional durability in the challenging underwater conditions.

Our study utilized two research vessels for the deployment and recovery of MSF devices. The first vessel was designated as the release vessel. It was anchored up-current of the turbine and equipped with the MSF samples, a magnet for activating the MSFs, a syringe with a needle for injecting water into balloons, release boards, balloon tags (which self-inflate after a time delay), a pressure transducer, a waterproof watch for timekeeping, a radio receiver with an antenna for signal detection, and portable two-way radios for communication with the recovery team in the second vessel. Additionally, waterproof field notebooks were used to record details such as release numbers, MSF serial numbers, frequency numbers, release and recovery times, and observations related to each deployment.

The release mechanism used for deploying the MSFs, shown in Fig. 6c, consisted of a spring-loaded body, spring tensioner, and latching hook assembly, which secured the MSF sample to a ballast weight line. The setup ensured a controlled release during deployment and maintained the desired depth until the balloon tags inflated to bring the MSF to the surface.

The second vessel served as the recovery vessel and was equipped with long-handled dip nets for capturing the MSFs, a magnet to deactivate them, buckets for storing inflated balloons, release boards, and MSF end caps. It also had a field computer equipped with the MSF Controller and a calibration file. The recovery team carried a radio receiver with an antenna to detect MSF radio frequency signals once the devices surfaced. Communication between the release and recovery crews was established prior to each MSF deployment for effective coordination.

Fig. 6d depicts the deployment crew releasing a MSF from the release vessel. Prior to deploying the actual MSF devices, preliminary tests were conducted using “dummy” MSFs to evaluate the release mechanism's effectiveness and refine the capture strategy using long-handled nets. These tests also helped determine the travel time of the MSFs through the turbine environment and reach the recovery crew.

Once the release mechanism's efficacy and the MSF's travel duration through the turbine environment were established, the deployment of actual MSFs began. Each MSF was programmed according to the travel time identified during the preliminary tests. Before deployment, recovery modules were attached to both ends of each MSF, along with balloon tags. To prepare the balloons, 5 mL of warm water was injected using a syringe and needle. The deployment time was marked by creating three acceleration spikes, generated by tapping the MSF against a hard surface. After passing through or near the turbine environment, the recovery module mechanism activated, releasing tungsten weights to increase the MSF's buoyancy, allowing it to rise near the water surface. The balloon tags then inflated a short time later, aiding in both buoyancy and visibility.

Once at the surface, the MSFs emitted radio signals, which were detected by the recovery crew positioned downstream of the tidal turbine. Upon detecting the signals and determining the approximate location, the recovery boat approached and captured each MSF using long-handled dip nets (Fig. 6e). A staff member then inspected each MSF for any physical damage. The data from each MSF were downloaded and analyzed to confirm data integrity. After verifying the validity of the collected samples, subsequent MSFs were released. This process was repeated on the second day of testing.

We released and recovered a total of 44 MSF samples over two days, from February 21 to 22, 2024. Each deployment was timed to coincide with peak tidal flows, with the MSFs released at the depths corresponding to the turbine's rotor-swept zone. This approach maximized the likelihood of interaction with the rotating blades, allowing the MSFs to capture real-time data on turbulence, shear stress, and pressure fluctuations. The release mechanism positioned the MSFs at precise depths, enabling multiple units to pass through or near the turbine blades and collect critical measurements in high-turbulence zones.

Out of 44 MSF releases, two direct blade strikes were captured on video by UW's underwater monitoring cameras, while all other trajectories passed near the turbine without contact. All 44 MSF releases were successfully recovered using the self-inflating balloon mechanism, which facilitated their ascent to the surface after completing their drift. The recovery crew, stationed downstream of the turbine, utilized handheld radio receivers and dip nets to locate and retrieve each unit.

To analyze data collected by the MSF, the Hydropower Biological Evaluation Toolset (HBET) was used (Hou et al., 2018). HBET processes the hydraulic characterization data from the MSF to predict potential

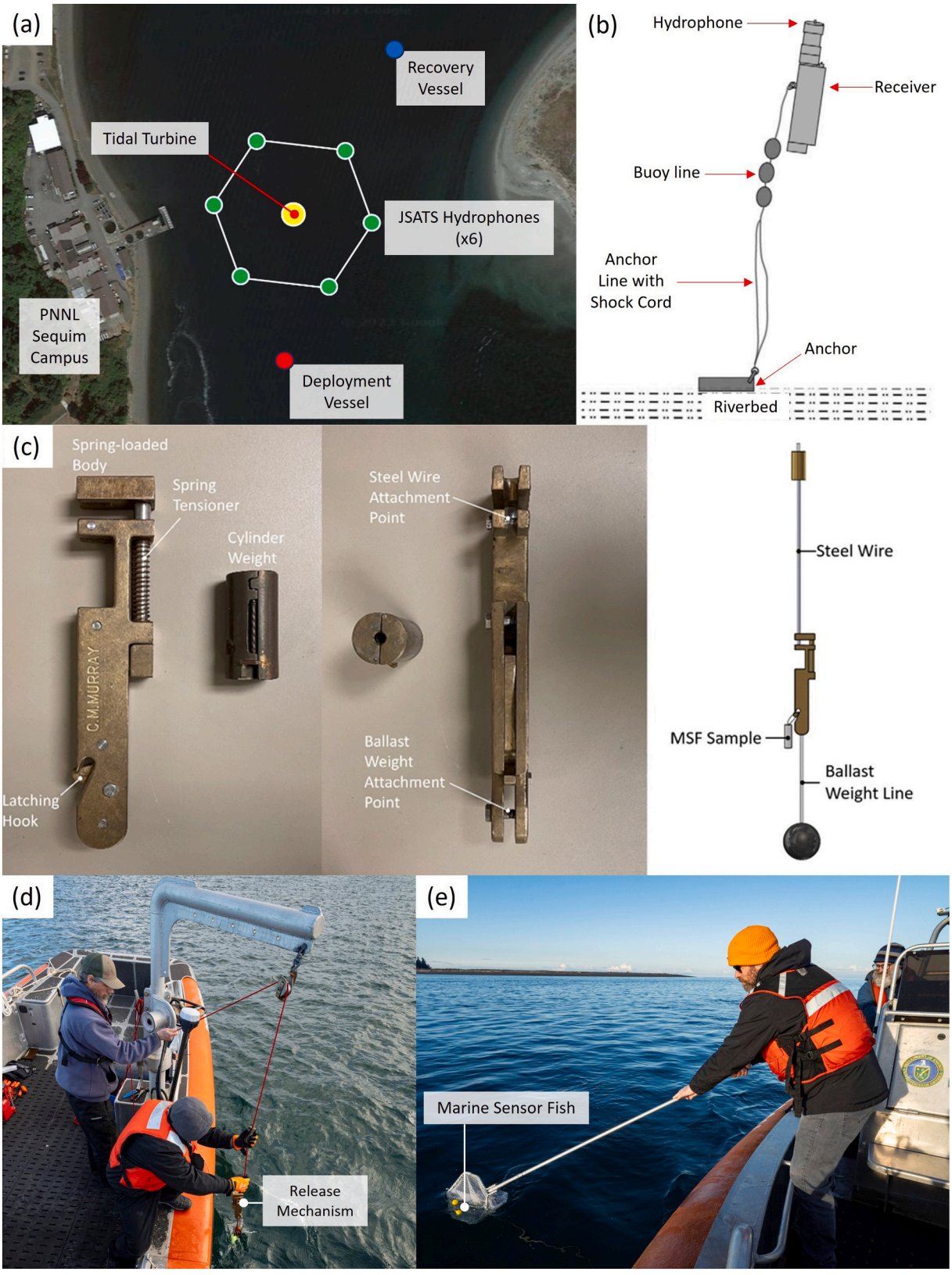

Fig. 6. Overview of the MSF deployment method near UW's tidal turbine at Sequim Bay Washington. (a) Map of the deployment location, showing the positioning of the UW tidal turbine (yellow dot), the JSATS hydrophones arranged in a hexagonal array (green dots), and the locations of the recovery (blue dot) and deployment (red dot) vessels. (b) Detailed schematic of the JSATS acoustic receiver mooring design, featuring the hydrophone, buoy line, and anchor system used to ensure stability and accurate data collection. (c) Release mechanism used for deploying the MSF. (d) Deployment crew releasing a MSF using the release mechanism. (c) Recovery team retrieving a MSF with fully inflated balloon tags using a long-handled dip net from the recovery vessel.

biological impacts on fish passing through turbines or other hydraulic structures, relating MSF data to known fish biological response relationships to estimate fish injury and mortality.

2.3.2. SF Mini deployment in scaled test rig models

This study used a scaled physical model of a Kaplan turbine within a hydraulic test rig, along with the SF Mini, to validate CFD simulations (Romero-Gomez et al., 2024b). The experimental setup involved systematically releasing and recovering SF Mini devices to measure critical hydraulic stressors, including pressure changes, collision events, and rotational velocities. The model featured a full-spiral intake, adjustable guide vanes, a five-blade runner, and a draft tube. A stainless-steel ingress pipe upstream of the turbine intake allowed precise control over sensor releases, while a fine-mesh net at the draft tube exit facilitated recovery. During deployments, the SF Mini, introduced into the intake flow via a booster pump, traveled through the distributor, runner, and draft tube, recording acceleration, angular velocity, and pressure. These modifications enabled efficient data collection without significantly interfering with flow conditions.

2.3.3. FSF laboratory testing

The FSF was tested in a flume tank at the Pacific Northwest National Laboratory (PNNL) to evaluate its performance under shear and strike conditions. The flume tank was equipped with a high-velocity shear nozzle to simulate extreme flow conditions. The FSF was exposed to a range of flow velocities and direct impacts with stationary structures, including turbine blade replicas. Sensors embedded in the FSF head, mid-body, and tail captured acceleration, rotational velocity, and shear forces. Each FSF unit underwent repeated testing to validate the consistency of data collection and assess durability under high-impact conditions.

3. Results

3.1. MSF field validation

During field deployment, a video recording captured the UW's tidal turbine blade striking the MSF (Fig. 7a). The corresponding sensor data (Fig. 7b) revealed a sudden acceleration spike exceeding 200 g, a rapid increase in rotational velocity up to 44 rad/s, and a sharp drop in pressure at the moment of impact. These responses were recorded within milliseconds of the collision, demonstrating the MSF's capability to capture transient, high-impact events. The data from this event displayed pronounced peaks in acceleration, rotational velocity, and pressure upon impact, highlighting the significant physical stressors that aquatic organisms may encounter near high-energy tidal devices. All MSF units were successfully retrieved with minimal damage, confirming the integrity of the collected data. The highest-pressure fluctuations were observed within 0.5 m of the rotor edge, identifying this area as a critical zone for potential fish impact.

3.2. SF Mini CFD validation

The SF Mini validated the CFD-generated flow fields, demonstrating strong alignment between the predicted and measured nadir pressures and rotational velocities. Fig. 8 provides an example of the SF Mini data collected, showing time-series plots of acceleration, rotational velocity, and pressure during turbine passage. These data highlight critical passage events, such as nadir pressures beneath the runner and elevated rotational velocity in turbulent regions, which closely correspond to CFD predictions (Romero-Gomez et al., 2024b). The results identified high-stress zones within the turbine environment, informing potential design optimizations aimed at reducing pressure gradients and minimizing collision-prone areas near the runner and distributor.

3.3. FSF laboratory testing

The shear flume tank used for testing is shown in Fig. 9a, while Fig. 9b captures the FSF being subjected to rapid shear flows. The devices were also tested against stationary structures (Fig. 9c and d), where the FSF experienced direct impacts with a stationary blade to evaluate its strike resilience. During these tests, data were collected from the head, mid-body, and tail regions of the FSF. An example dataset, shown in Fig. 9e, illustrates a shear event caused by jet flow. The data plots highlight a rapid acceleration spike, with values reaching approximately 20 g across all body regions, followed by an increase in rotational velocity of up to 8 rad/s. Pressure fluctuations during these events remained relatively stable, with transient peaks around 140 kPa.

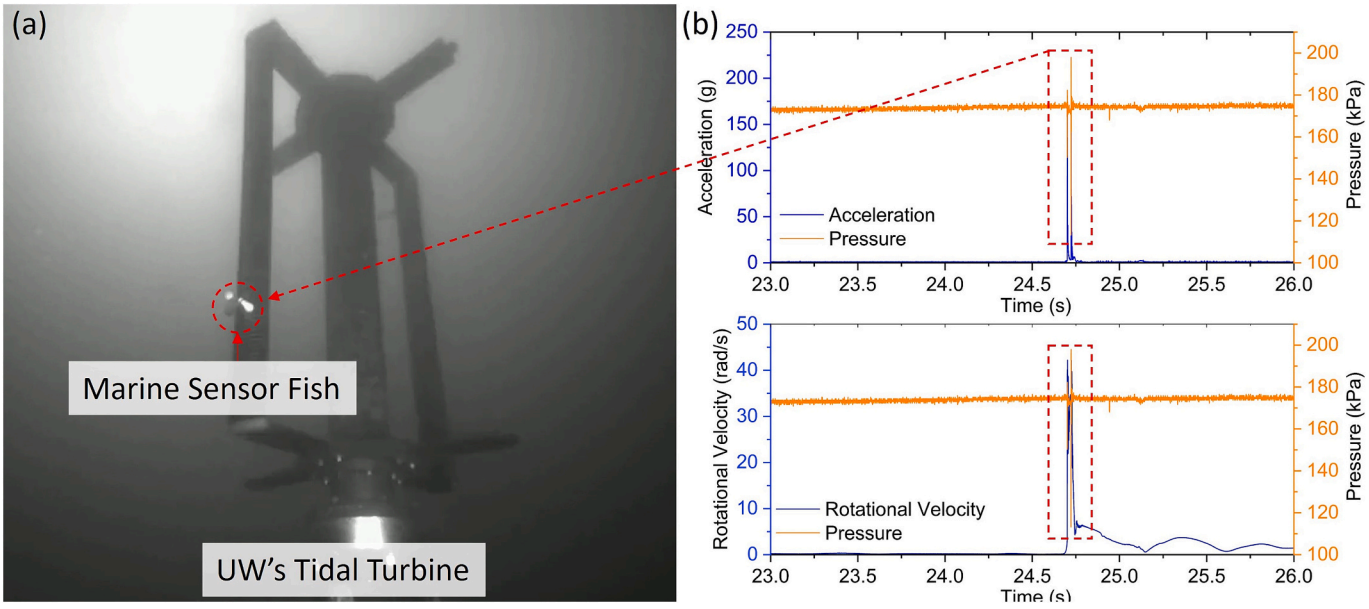

Fig. 7. (a) Screen capture from video footage showing UW's tidal turbine blade striking an MSF in Sequim Bay. (b) Corresponding data from the strike, illustrating peaks in acceleration, rotational velocity, and pressure at the moment of impact. The photo and video footage are courtesy of Dr. Christopher Bassett of the UW.

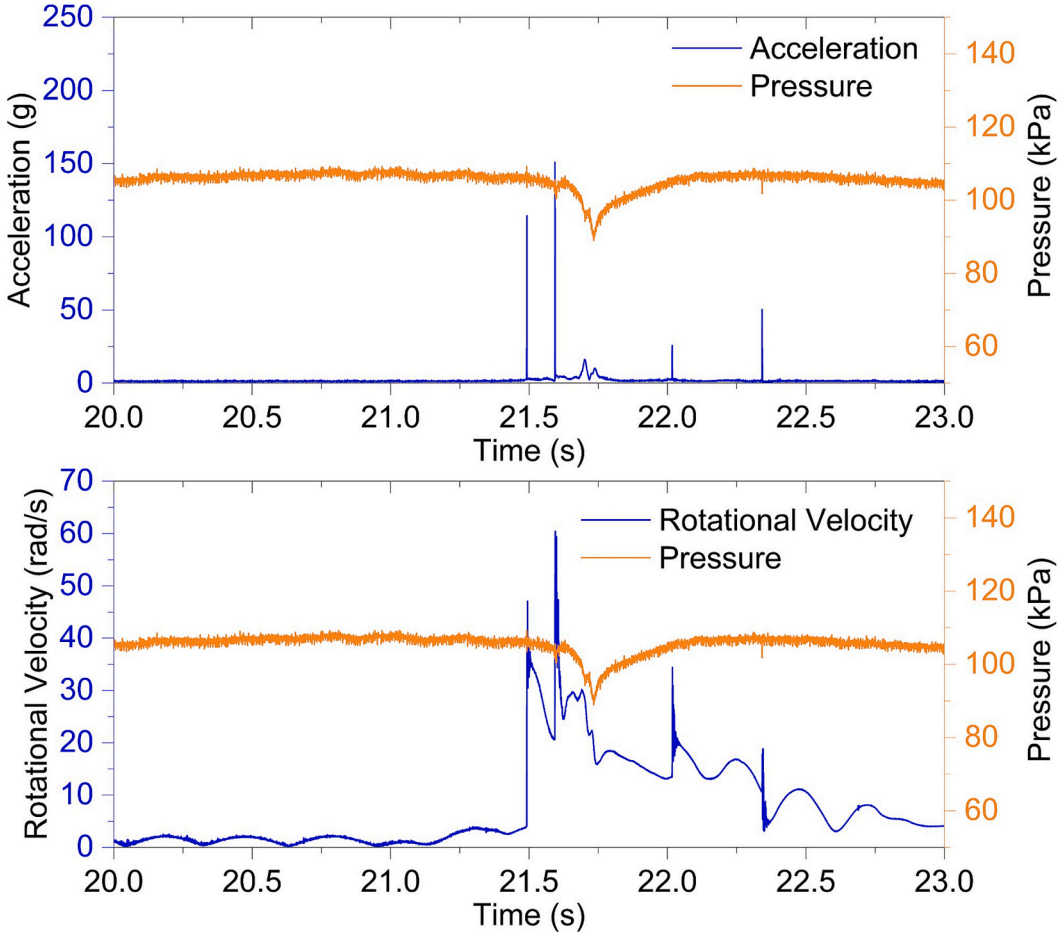

Fig. 8. Example of SF Mini data collected from a scaled model of a Kaplan turbine in a test rig. The data are compared with CFD simulations to validate flow characteristics and assess hydraulic performance.

4. Discussion

The findings from the MSF field validation in Sequim Bay highlight the potential physical stressors present near tidal turbine systems, particularly within the rotor-swept zone. The MSF recorded extreme conditions, including high acceleration forces exceeding 200 g and rapid rotational velocities reaching 44 rad/s, within 0.5 m of the turbine blade edge. These results indicate potential risks posed to aquatic organisms in high-energy environments, where such forces may lead to injury or disorientation. These risk zones demand careful attention in turbine design to reduce turbulence and shear forces that could negatively impact aquatic habitats.

Similarly, a recent study observed that salmon smolt exhibited signs of disorientation while navigating the rotor-swept area of the ORPC riverine turbine in Igiugig, Alaska, with some fish experiencing direct blade impacts (Courtney et al., 2022). These observations align with the MSF field validation findings, where high-intensity turbulence and shear stresses were recorded in the rotor-swept zone, suggesting comparable risks to fish, including disorientation and collision. Together, these findings emphasize the importance of empirical data in identifying high-risk areas and informing design adjustments that can reduce injury risks for aquatic species in operational MRE systems.

The SF Mini study demonstrated the capability of high-resolution data to validate computational predictions for hydropower turbine design. Deployed in a controlled Kaplan turbine model, the SF Mini captured critical hydraulic metrics, such as nadir pressure and rotational velocity spikes, which were consistent with CFD predictions. This integration of empirical data and computational methods highlights its value in refining turbine designs to enhance fish passage safety and minimize ecological impacts. By supporting the development of more sustainable turbine designs, this approach demonstrates the importance of high-resolution measurements in improving simulation accuracy. Comparing observed physical data with CFD predictions allows for iterative refinements to the models, enhancing their reliability and ensuring they effectively replicate real-world dynamics (Gao et al., 2023; Gao et al., 2024).

Building on this focus on fish passage safety, laboratory experiments conducted with the FSF provided data on the physical forces aquatic organisms may encounter when interacting with hydropower and MRE systems. By simulating controlled strikes along three critical body regions such as the head, mid-body, and tail, the FSF captured detailed measurements of acceleration, rotational velocity, and pressure fluctuations during impact events. Peak acceleration values exceeded 20 g across all body regions, with the head region experiencing the most pronounced spikes. Rotational velocities during collisions reached approximately 8 rad/s, highlighting the significant mechanical forces aquatic species are subjected to in these high-energy environments. Although pressure fluctuations were less variable than acceleration or rotational velocity, transient peaks during impacts revealed localized stress events that may contribute to fish injury.

These results illustrate the FSF's capability to simulate the biomechanical responses of fish bodies under collision scenarios, enabling a deeper understanding of the mechanical stressors affecting different body regions. The data suggest that the head and mid-body regions are particularly vulnerable to high-impact forces, potentially leading to injury or mortality during interactions with turbine blades or other high-

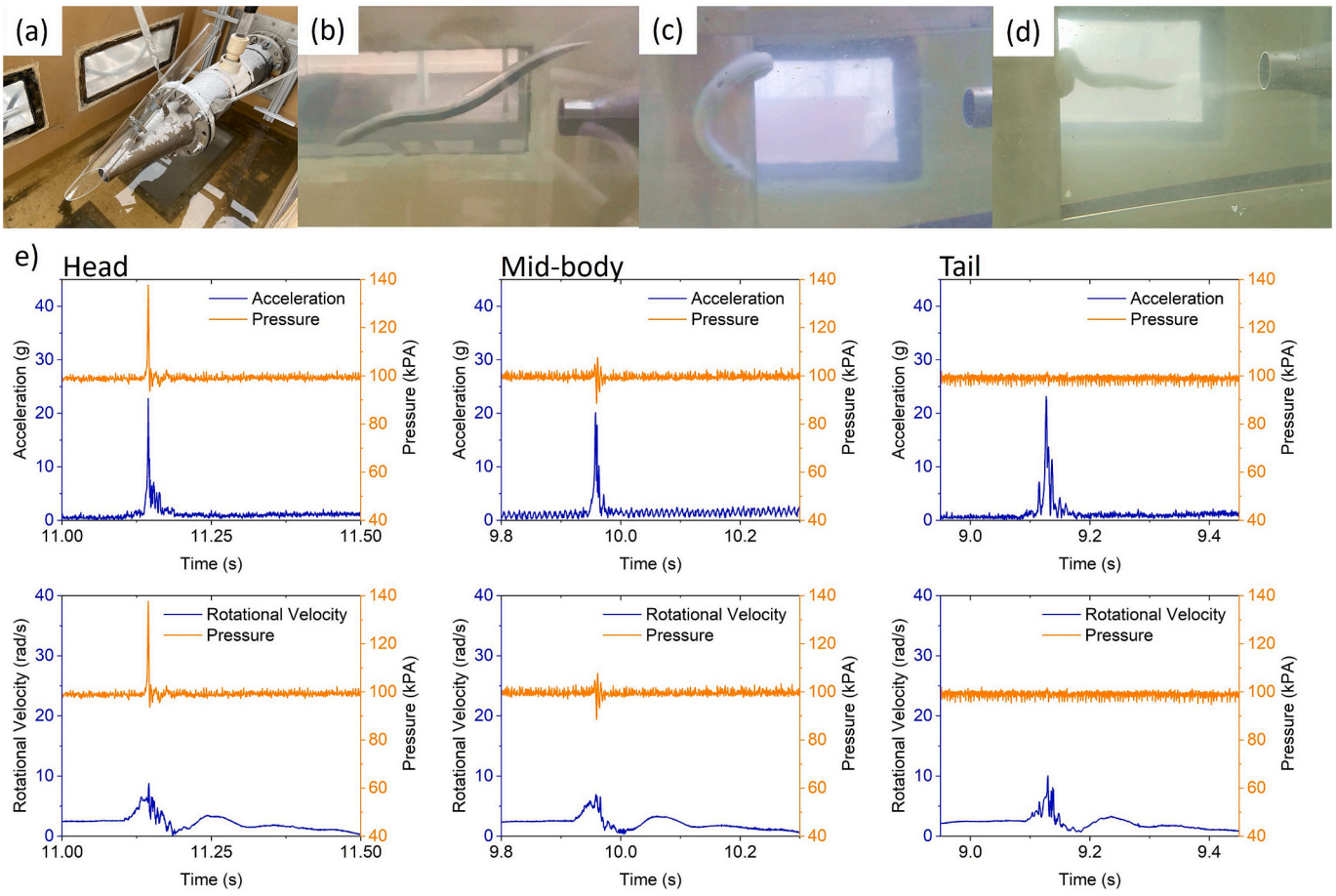

Fig. 9. (a) Photograph of the shear flume tank where the FSE was launched for shear and strike testing. (b) Photograph of the FSE subjected to rapid shear flows. (c and d) Photographs of the FSE showing a direct blow on a stationary blade. (e) Example of FSE data plots for the head, mid-body, and tail regions, showing a shear event caused by jet flow, where rapid acceleration was followed by an increase in rotational velocity, indicating exposure to a high shear zone.

energy components. Such findings are instrumental for identifying critical risk zones and guiding the development of fish-friendly turbine designs that minimize acceleration and rotational velocity peaks near these areas, thereby reducing the likelihood of severe impacts.

The combined findings from the sensor devices show their effectiveness in capturing the key physical stressors aquatic organisms face in both natural and engineered systems. This research establishes a strong foundation for improving the design and operation of MRE and hydropower systems, ensuring their development aligns with environmental sustainability goals. However, several limitations of the current devices must be addressed to further enhance their capabilities. The lack of real-time data transmission requires physical retrieval for analysis, which can be impractical for large-scale or extended deployments. Additionally, the limited recording durations, 584 s for the MSF and 292 s for the SF Mini and FSF. constrain their use in long-term studies. Deployments in remote or extreme environments, such as offshore MRE systems far from land, also pose significant logistical challenges, as the convenience of the Sequim Bay site near the PNNL campus may not always be replicable.

Future studies should address these limitations by integrating telemetry for real-time monitoring, extending battery life and data storage capacity for longer recording durations, and developing robust recovery mechanisms for remote deployments. Furthermore, combining these advancements with other technologies, such as imaging systems, could further enhance the understanding of fish-turbine interactions and inform adaptive management strategies for aquatic ecosystems.

5. Conclusion

The comprehensive development and testing of SF variants, including the MSF, SF Mini, and FSF, have demonstrated their ability to collect precise, high-resolution data on fish passage conditions and hydrodynamic stressors in marine and hydropower environments. The MSF was validated through field deployments at a tidal turbine in the Salish Sea, successfully capturing critical forces such as shear stress, pressure changes, and collision impacts near operational MRE devices. The SF Mini effectively evaluated flow conditions in a scaled physical model of a bypass design, providing valuable data to validate CFD models and enhance fish passage safety. Similarly, the FSF underwent rigorous shear and strike testing under laboratory conditions, verifying its durability and ability to replicate the physical impacts experienced by fish in turbulent environments. These advantages make the SF technology a powerful tool for advancing research on fish-turbine interactions and informing the design of safer, environmentally sustainable energy systems.

Future efforts will focus on addressing current limitations to enhance the utility of these devices. Integrating telemetry systems for real-time data transmission, extending battery life and storage capacity for longer recording durations, and improving recovery mechanisms for deployments in remote or extreme environments will significantly expand their applicability. These advancements, combined with expanded field studies and the integration of advanced monitoring tools such as imaging systems, will further enhance the SF technology's capability to support adaptive management strategies for aquatic ecosystems.

The data gathered thus far provide a strong foundation for reducing biological and environmental impacts and enhancing turbine designs to improve safety and functionality. Continued refinements and technological advancements will be critical for ensuring the development of environmentally sustainable energy solutions while minimizing risks to aquatic life.

CRediT authorship contribution statement

Aljon Salalila: Writing – original draft, Visualization, Methodology, Investigation, Formal analysis, Data curation. **Jun Lu:** Writing – review & editing, Methodology, Investigation, Formal analysis. **Jayson J. Martinez:** Writing – review & editing, Validation, Methodology, Investigation. **Hongfei Hou:** Writing – review & editing, Software, Methodology, Investigation. **Zhiqun Daniel Deng:** Writing – review & editing, Supervision, Project administration, Methodology, Investigation, Funding acquisition, Conceptualization.

Declaration of competing interest

Zhiqun Daniel Deng reports financial support was provided by US Department of Energy Water Power Technologies Office and Office of Technology Transitions. If there are other authors, they declare that they have no known competing financial interests or personal relationships that could have appeared to influence the work reported in this paper. The SF Mini was patented (11533818 and 12144139).

Acknowledgement

This research was funded by the U.S. Department of Energy Water Power Technologies Office and Office of Technology Transitions. The authors would like to thank Natel Energy, UW, the U.S. Army Corps of Engineers, and the Farmers Conservation Alliance for their collaboration and support. Special thanks to Dr. Pedro Romero-Gomez of Andritz Hydro for providing the SF Mini data, and to Dr. Christopher Bassett of UW for facilitating the use of the tidal turbine and sharing video footage of the MSF passing through the turbine. The authors also sincerely thank the staff at PNNL for their assistance with the manufacturing and deployment of the MSF.

Data availability

Data will be made available on request.

References

Amaral, S., Bevelhimer, M., Cada, G., Giza, D., Jacobson, P., McMahon, B., Pracheil, B., 2015. Evaluation of behavior and survival of fish exposed to an axial-flow hydrokinetic turbine. N. Am. J. Fish. Manage. 35 (1), 97–113. https://doi.org/10.1080/02755947.2014.982333.

Bender, A., Langhamer, O., Francisco, F., Forslund, J., Hammar, L., Sundberg, J., Molander, S., 2023. Imaging-sonar observations of salmonid interactions with a vertical axis instream turbine. River Res. Appl. 1–12, Art. no. RRA.4171. https://doi.org/10.1002/rra.4171.

Boys, C.A., Pflugrath, B.D., Mueller, M., Pander, J., Deng, Z.D., Geist, J., 2018. Physical and hydraulic forces experienced by fish passing through three different low-head hydropower turbines. Mar. Freshw. Res. 70 (9), 1274–1283. https://doi.org/10.1071/MF18100.

Brown, R.S., et al., 2014. Understanding barotrauma in fish passing hydro structures: a global strategy for sustainable development of water resources. Fisheries 39 (3), 108–122. https://doi.org/10.1080/03632415.2014.883570.

Copping, A., Battey, H., Brown-Saracino, J., Massaua, M., Smith, C., 2014. An international assessment of the environmental effects of marine energy development. Ocean Coast. Manage. 99, 3–13. https://doi.org/10.1016/j.ocecoaman.2014.04.002.

Copping, A., Hemery, L., Viehman, H., Seitz, A., Staines, G., Hasselman, D., 2021. Are fish in danger? A review of environmental effects of marine renewable energy on fishes. Biol. Conserv. 262, Art. no. 109297. https://doi.org/10.1016/j.biocon.2021.109297.

Copping, A., Hasselman, D.J., Bangley, C.W., Culina, J., Carcas, M., 2023. A probabilistic methodology for determining collision risk of marine animals with tidal energy turbines. J. Mar. Sci. Eng. 11, no. 11, Art. no. 2151. https://doi.org/10.3390/jmse11112151.

Cotter, E., Staines, G., 2023. Observing fish interactions with marine energy turbines using acoustic cameras. Fish Fish. 24 (3), 1–14. https://doi.org/10.1111/faf.12782.

Courtney, M., Flanigan, A., Hostetter, M., Seitz, A., 2022. Characterizing sockeye salmon smolt interactions with a hydrokinetic turbine in the Kvichak River, Alaska. N. Am. J. Fish. Manage. 42 (4), 1054–1065. https://doi.org/10.1002/nafm.10806.

Deng, Z., Carlson, T.J., Duncan, J.P., Richmond, M.C., Dauble, D.D., 2010. Use of an autonomous sensor to evaluate the biological performance of the advanced turbine at Wanapum dam. J. Renewable Sustainable Energy 2, no. 5, Art. no. 053104. https://doi.org/10.1063/1.3501336.

Deng, Z.D., et al., 2014. Design and implementation of a new autonomous sensor fish to support advanced hydropower development. Rev. Sci. Instrum. 85, no. 11, Art. no. 115001. https://doi.org/10.1063/1.4900543.

Deng, Z.D., Salalila, A., Copping, A.E., Martinez, J.J., Li, Y., 2024. Environmental monitoring and risk assessment for marine energy systems. In: Encyclopedia of Renewable Energy, Sustainability and the Environment, 2nd ed vol. 3. Elsevier, pp. 141–150. https://doi.org/10.1016/B978-0-323-93940-9.00263-2.

Gao, Y., Yu, Z., Huang, L., Zeng, Y., Liu, X., Tang, D., 2023. Photoinduced electron transfer modulated photoelectric signal: toward an organic small molecule-based photoelectrochemical platform for formaldehyde detection. Anal. Chem. 95 (9), 9130–9137. https://doi.org/10.1021/acs.analchem.3c01690.

Gao, Y., Tang, J., Zhou, Q., Yu, Z., Wu, D., Tang, D., 2024. Excited-state intramolecular proton transfer-driven photon-gating for photoelectrochemical sensing of CO-releasing molecule-3. Anal. Chem. 96 (12), 5014–5021. https://doi.org/10.1021/acs.analchem.4c00324.

L. Garavelli, A. E. Copping, L. G. Hemery, and M. C. Freeman, Eds., OES-Environmental 2024 State of the science report: environmental effects of marine renewable energy development around the world. Report for Ocean Energy Systems (OES), Sept. 2024. doi:https://doi.org/10.2172/2438585.

D. J. Hasselman et al., "Scaling up our understanding of environmental effects of marine renewable energy development from single devices to large-scale commercial arrays," Sci. Total Environ., vol. 904, Sept. 2023, Art. no. 166801, doi:https://doi.org/10.1016/j.scitotenv.2023.166801.

Heisey, P.G., Mathur, D., Rineer, T., 1992. A reliable tag–recapture technique for estimating turbine passage survival: application to young-of-the-year American Shad (Alosa sapidissima). Can. J. Fish. Aquat. Sci. 49 (9), 1826–1834. https://doi.org/10.1139/f92-202.

L. G. Hemery et al., "Animal displacement from marine energy development: Mechanisms and consequences," Sci. Total Environ., vol. 917, Jan. 2024, Art. no. 170390, doi:https://doi.org/10.1016/j.scitotenv.2024.170390.

Hou, H., Deng, Z.D., Martinez, J.J., Fu, T., Duncan, J.P., Johnson, G.E., Lu, J., Skalski, J. R., Townsend, R.L., Tan, L., 2018. A hydropower biological evaluation toolset (HBET) for characterizing hydraulic conditions and impacts of hydro-structures on fish. Energies 11, no. 4, Art. no. 990. https://doi.org/10.3390/en11040990.

L. Kilcher, M. Fogarty, and M. Lawson, "Marine Energy in the United States: An Overview of Opportunities," Nat. Renew. Energy Lab., Golden, CO, USA, Tech. Rep. NREL/TP-5700-78773, Feb. 2021. [Online]. Available: https://www.nrel.gov/docs/fy21osti/78773.pdf.

Lu, J., Deng, Z.D., Li, H., Myjak, M.J., Martinez, J.J., Xiao, J., Brown, R.S., Cartmell, S.S., 2016. A small long-life acoustic transmitter for studying the behavior of aquatic animals. Rev. Sci. Instrum. 87, no. 11, Art. no. 114902. https://doi.org/10.1063/1.4967941.

Martinez, J., Deng, Z.D., Tian, C., Mueller, R., Phonekhampheng, O., Singhanouvong, D., Thorncraft, G., Phommavong, T., Phommachand, K., 2019a. In situ characterization of turbine hydraulic environment to support development of fish-friendly hydropower guidelines in the lower Mekong River region. Ecol. Eng. 133, 88–97. https://doi.org/10.1016/j.ecoleng.2019.04.028.

Martinez, J.J., Deng, Z.D., Titzler, P.S., Duncan, J.P., Lu, J., Mueller, R.P., Tian, C., Trumbo, B.A., Ahmann, M.L., Renholds, J.F., 2019b. Hydraulic and biological characterization of a large Kaplan turbine. Renew. Energy 131, 240–249. https://doi.org/10.1016/j.renene.2018.07.034.

Peraza, J.I., Horne, J.K., 2023. Quantifying conditional probabilities of fish-turbine encounters and impacts. Front. Mar. Sci. 10, Art. no. 1270428. https://doi.org/10.3389/fmars.2023.1270428.

Polagye, B., Bassett, C., Scott, M., Cotter, E., Joslin, J., Jones, L., Talpey, G., Snortland, A., Peraza, J., Horne, J., July 2024. ALFA Task 10: Quantifying Collision Risk for Fish and Turbines. Univ. of Washington, Seattle, WA, USA. https://doi.org/10.2172/2438503. Rep. DE-EE-0006816.0000,.

Richmond, M.C., Serkowski, J.A., Ebner, L.L., Sick, M., Brown, R.S., Carlson, T.J., 2014. Quantifying barotrauma risk to juvenile fish during hydro-turbine passage. Fisheries Res. 154, 152–164. https://doi.org/10.1016/j.fishres.2014.01.007.

Romero-Gomez, P., Poomchaivej, T., Razdan, R., Robinson, W., Peyreder, R., Raeder, M., Baumgartner, L.J., 2024a. Sensor fish deployments at the Xayaburi hydropower plant: measurements and simulations. Water 16, no. 5, Art. no. 775. https://doi.org/10.3390/w16050775.

Romero-Gomez, P., Salalila, A., Deng, Z.D., Peyreder, R., 2024b. Feasibility study for test rig assessments of fish passage conditions in a Kaplan turbine. Heliyon 10, Art. no. e26846. https://doi.org/10.1016/j.heliyon.2024.e26846.

Salalila, A., Deng, Z.D., Martinez, J.J., Lu, J., Baumgartner, L.J., 2019. Evaluation of a fish-friendly self-cleaning horizontal irrigation screen using autonomous sensors. Mar. Freshw. Res. 70 (9), 1274–1283. https://doi.org/10.1071/MF19194.

Salalila, A., Martinez, J., Tate, A., Acevedo, N., Salalila, M., Deng, Z.D., 2023. Optimizing balloon tag assembly to recover sensor fish and live fish. J. Vis. Exp. no. 200, Art. no. e65632. https://doi.org/10.3791/65632.

Shen, H., Zydlewski, G.B., Viehman, H.A., Staines, G., 2016. Estimating the probability of fish encountering a marine hydrokinetic device. Renew. Energy 97, 746–756. https://doi.org/10.1016/j.renene.2016.06.026.

Weiland, M.A., Deng, Z.D., Seim, T.A., LaMarche, B.L., Choi, E.Y., Fu, T., Carlson, T.J., Thronas, A.I., Eppard, M.B., 2011. A cabled acoustic telemetry system for detecting and tracking juvenile salmon: part 1. Engineering design and instrumentation. Sensors 11 (6), 5645–5660. https://doi.org/10.3390/s110605645.

Yoshida, T., Furuichi, D., Williamson, B.J., Zhou, J., Dong, S., Li, Q., Kitazawa, D., 2022. Experimental study of fish behavior near a tidal turbine model under dark conditions. J. Mar. Sci. Technol. 27 (4), 541–548. https://doi.org/10.1007/s00773-021-00850-w.